21st Australasian Fluid Mechanics Conference
Adelaide, Australia
10-13 December 2018

Development of a Verification Methodology for Large-Eddy Simulation of Underexpanded Natural Gas Jets

M. R. Yosri[1], J. S. Lacey[1], M. Talei[1], R. L. Gordon[1] and M. J. Brear[1]

[1]Department of Mechanical Engineering
The University of Melbourne, Parkville 3010, Australia

Abstract

Direct injection (DI) of compressed natural gas (CNG) in spark-ignited, internal combustion engines has the potential to improve efficiency and reduce CO_2 emissions compared to gasoline-fueled equivalents. In order to realise these benefits, a thorough understanding of the DI CNG process is required. DI CNG features compressible, supersonic gaseous jets which have a complex flow field with shocks and discontinuities that affect air/fuel mixing. This paper presents large-eddy simulation (LES) of two nozzle geometries [5, 15] to study the flow characteristics of highly underexpanded compressed natural gas jets and the effects of changing the ratio of the nozzle total pressure (P_0) to the ambient static pressure (P_∞), defined as nozzle pressure ratio (NPR) ranging from 6.5 to 8.5. Several quantities are then examined to verify the fidelity of the LES results. The transient development of the highly underexpanded natural gas jets is examined and the location and width of the Mach disk are compared with the literature data and empirical relations. Additionally, the formation process of the intersection of a strong normal shock close to the nozzle exit, referred to as the Mach disk and its intersection with oblique shocks known as the triple point are discussed.

Introduction

Compressed Natural gas (CNG) is commonly used as an alternative fuel for different applications due to energy-specific low carbon emissions, attractive cost, availability, high antiknock resistance and extended lean flammability [9]. Port fuel injection (PFI) and direct injection (DI) are two typical injection methods in natural gas engines. However, DI CNG engines tend to have improved volumetric efficiency and torque capability over PFI equivalents [9]. As the major component of the CNG is methane (CH_4), which has a lower density compared with other conventional fuels, natural gas DI engines need to feature high injection pressure to achieve homogeneous air/fuel mixing and fast distribution of natural gas in the combustion chamber [13].

One parameter used to characterise natural gas injection is the nozzle pressure ratio (NPR). Donaldson and Snedeker [3] performed a parametric study of the impact of varying NPR on the structure of gaseous jets. They showed that depending on the NPR, the gas jet has a transition from a subsonic jet to moderately under-expanded and eventually highly under expanded gaseous jet. As DI CNG engines with purpose-built injection hardware have a fuel rail pressure ranging from approximately $16-20bar$ injected into a cylinder with pressure from $0.4bar$ to $4bar$, generally the NPR is more than 4.05 and categorised as a highly underexpanded gaseous jet [5].

Recently, advancements in computing power have made LES of complex flows feasible. This has the advantage of capturing details of supersonic flows with numerous expansion shocks more accurately than Reynolds-averaged Navier Stokes (RANS) calculations. Vuorinen et. al [15, 14] investigated the effect of NPR on gas jet features including Mach disk height, Mach disk width, penetration length and volumetric growth of the jet. They observed that all the aforementioned parameters will increase by enhancing NPR. Hamzehloo and Aleiferis [5, 6] conducted various studies to understand transient, highly underexpanded gas jets and their development characteristics with several fuels (hydrogen and methane) and various NPR. They encountered concave flow profiles at the beginning of injection that rolled up to the top of the jet, helping to initiate a vortex ring. They observed that a three dimensional vortex ring is formed when a low density gas was injected to a high density environment or a cold gas entered a hot media. Furthermore, they showed that $20\mu s$ after the start of injection (ASOI), the vortex ring merges into the shear layer and helps to increase air/fuel mixing characteristics.

A few studies [4, 10] have been conducted to determine the effect of nozzle geometry and diameter on downstream flow characteristics of highly under expanded gas jets. Dong et al. [4] investigated injection processes and shock wave characteristics by using schlieren imaging for different NPRs and nozzle diameters. They showed that the Mach disk height increased by enhancing nozzle diameter. In addition, Mach disk height reached to a maximum value of $5ms$ ASOI and remained constant for $10ms$, thenceforth it continued to decrease. In a numerical study, Li et al. [10] investigated the effect of different nozzle geometries (circular, elliptic, square and rectangular) on the jet characteristics and showed that square nozzle lead to the fastest penetration. However, the Mach disk location is the same for various shapes. In addition, they defined mixing area the iso-line of gas jet $Y_F = 2\%$ (fuel mass fraction) and found that the elliptic jet had the largest mixing area.

At this point, the existing literature has not captured how the internal geometry and the flow inside an injector can impact the resulting highly underexpanded gaseous jets. In this paper, the formation process of the triple point and Mach disk is investigated for two different internal nozzle geometries.

Numerical Methodology

In this study, the CONVERGE CFD software package is used as a computational framework for the LES study of highly underexpanded gaseous jets with Reynolds number in order of 10^5 [12]. CONVERGE uses the finite volume method to solve the conservation equations with a second order Monotonic Upstream-Centered Scheme (MUSCL) for spatial discretisation. A step flux limiter is used for shock wave treatment [12]. The pressure implicit with splitting of operators (PISO) algorithm is implemented to solve governing equations [8]. Simulation with a variable time step is calculated based on maximum of the Courant Friedrich Lewy (CFL) number (convection, diffusion and Mach number). The time step varied from $1e^{-9}s$ to $5e^{-8}s$ with the total simulation of $500\mu s$. Moreover, the Schmidt number of the flow is set to $Sc = 0.78$ and the Prandtl number is $Pr = 0.78$.

Computational Domain

In the present study, 3D simulations of two different wall bounded closed systems were performed from the previous works (see figure 1). Both systems have a low pressure tank full of nitrogen $P_\infty = 1bar$. and two different high pressure methane tanks with pressures of $P_0 = 6.5bar$ and $8.5bar$. The main difference between the two geometries is that in Geometry I there is a long tube ($\approx 17D$) with the diameter of the exit nozzle between the high and low pressure tanks and in Geometry II, there is a short tube ($\approx 1.6D$) between the two pressure zones.

The methane gas jet into nitrogen in both geometries is hypersonic, therefore the effect of viscosity on the high pressure tank walls is negligible and slip wall condition can be assumed. However, for the low pressure tank walls, the no slip boundary condition is applied. The initial temperature of the entire domain and the walls is $T = 298K$.

In order to reduce the computational cost, the adaptive mesh refinement (AMR) algorithm [12] is used. In this study, AMR algorithm is able to refine the mesh where gradient of a velocity field has large values. The base grid size of this study is $D/2$ and the smallest grid size is $D/32$ which is consistent with literature [5, 15]. Furthermore, the total number of cells is limited to $10,000,000$ overall mesh size.

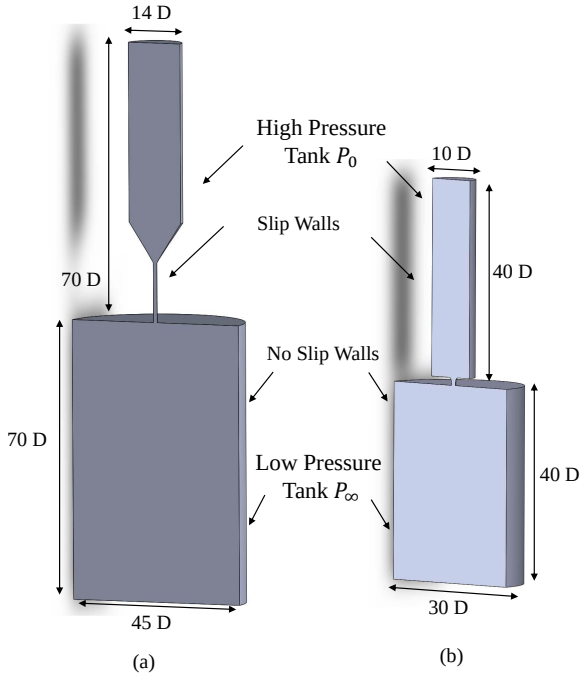

Figure 1: Sectional view of the computational domain a) Geometry I - Ref. [15] and b) Geometry II - Ref [5]. The variable D is the diameter of nozzle.

Dynamic Structure LES

The governing and transport equations for LES are decomposed into resolved terms and sub-grid scale (SGS) models. The decomposition method is based on spatial filtering instead of the time-averaging used in RANS. For compressible flows, Favre averaged quantities defined as

$$\widetilde{\phi_i} = \frac{\overline{\rho\phi_i}}{\overline{\rho}}, \tag{1}$$

are used. The momentum equitation is used here to explain the LES decomposition technique:

$$\frac{\partial\overline{\rho}\widetilde{u_i}}{\partial t} + \frac{\partial\overline{\rho}\widetilde{u_i}\widetilde{u_j}}{\partial x_j} = -\frac{\partial\overline{P}}{\partial x_i} + \frac{\partial\overline{\sigma_{ij}}}{\partial x_j} - \frac{\partial\tau_{ij}}{\partial x_j}, \tag{2}$$

where the ρ is the density of mixture, u is the velocity, P detonates pressure and $\overline{\sigma_{ij}}$ is the resolved shear stress tensor. The sub-grid stress terms can be calculated by,

$$\tau_{ij} = \overline{\rho}(\widetilde{u_i u_j} - \widetilde{u_i}\widetilde{u_j}). \tag{3}$$

The SGS terms such as τ_{ij} cannot be computed directly from the equations and they should be modelled. In this study, the one equation non-viscosity based dynamic structure model is used [11]. In this method, one extra equation for turbulent kinetic energy is solved,

$$\frac{\partial\overline{\rho}k}{\partial t} + \frac{\partial\overline{\rho}\widetilde{u_j}k}{\partial x_j} = \frac{\partial(\frac{\mu}{Pr_{sgs}}\frac{\partial k}{\partial x_j})}{\partial x_j} + \tau_{ij}\overline{S_{ij}} - \rho\varepsilon, \tag{4}$$

where, Pr_{sgs} is set to be 0.78, μ is dynamic viscosity, S_{ij} detonates the filtered strain rate tensor, k is the sub-grid kinetic energy and ε is the sub-grid dissipation rate which can be calculated as follows:

$$\overline{S_{ij}} = \frac{1}{2}(\frac{\partial\widetilde{u_i}}{\partial x_j} + \frac{\partial\widetilde{u_j}}{\partial x_i}), \tag{5}$$

$$k = \frac{1}{2}(\overline{\rho}(\widetilde{u_i u_i} - \widetilde{u_i}\widetilde{u_i})), \tag{6}$$

$$\varepsilon = C_\varepsilon\frac{k^{1.5}}{\Delta}. \tag{7}$$

The variable C_ε is a model constant and Δ is the grid size. Akira and Kiyosi [1] showed that, in order to prevent the overestimation of the sub-grid dissipation rate, C_ε is ≈ 1. The SGS stress tensor τ_{ij} can be calculated as follows:

$$\tau_{ij} = 2k\overline{\rho}\frac{L_{ij}}{L_{ii}}. \tag{8}$$

The Leonard stress term, L_{ij}, can be computed using equation 9.

$$L_{ij} = \widehat{\widetilde{u_i}\widetilde{u_j}} - \widehat{\widetilde{u_i}}\widehat{\widetilde{u_j}} \tag{9}$$

The "$\widehat{\ }$" sign indicates an additional spatial test filter which is twice the grid size.

Further details on remaining governing equations can be found in Ref [12].

Result and Discussion

The flow field after the nozzle exit can be characterised using parameters such as Mach disk location (H_{disk}) and the width of the Mach disk (W_{disk}). The parameter H_{disk} is the distance from the strong normal shock location to the nozzle exit and W_{disk} is the width of this normal shock. A frequently used empirical correlation (proposed by Sherman [2]) is employed to calculate the Mach disk location.

Geometry s	NPR	H_{disk}/D	Error I	Error II	W_{disk}/D	Error I
Geometry I	6.5	1.64	1.8%	-4.1%	0.42	-8.6%
	8.5	1.91	-2.7%	-2.3%	0.62	-8.8%
Geometry II	6.5	1.71	-3.2%	2.2%	0.65	-5.2%
	8.5	2.07	-4.8%	0.8%	0.78	-8.9%

Table 1: Mach disk location and width; Error I is the difference between the LES in the present work and each nozzle geometry in the related literature, and Error II is difference between the current simulation work and the empirical relation.

$$H_{disk}/D = 0.67 * \sqrt{NPR} \tag{10}$$

The Mach disk location obtained from our simulations and that reported in the previous studies, are compared with the result of the empirical correlation. In table 1 for both nozzle geometries and across all NPRs, the difference between the H_{disk} obtained from our simulations and that from previous works is less than 5%. Since there is no unique correlation for W_{disk}, we therefore compare this parameter with that reported in previous works. As shown in table 1, for a given NPR, the difference between two different geometries is slightly higher but less than 10%. One possible reason could be that the sub-grid scale model of previous works is different with that used in the current study. In addition, by increasing the NPR in both Geometries, H_{disk} and W_{disk} increase and they are consistent with the literature and equation 10.

Furthermore, it is interesting to note that for a given NPR, the internal geometry influences the Mach disk location (H_{disk}/D) and Mach disk width (W_{disk}/D).

Another empirical correlation from Hill and Ouellete [7] is used to assess the fidelity of our simulation. Hill and Ouellete showed that the penetration length (Z_{tip}) can be determined by:

$$Z_{tip} = \Pi(\frac{M}{\rho_\infty})^{1/4} t^{1/2}, \tag{11}$$

where ρ_∞ is the downstream density, Π indicates a scaling constant, ($\Pi \approx 3$ for the round jets), and M is the momentum of gaseous flow rate. Figure 2 shows that there is less than a 5% difference between our results and those obtained from Hill and Ouellete.

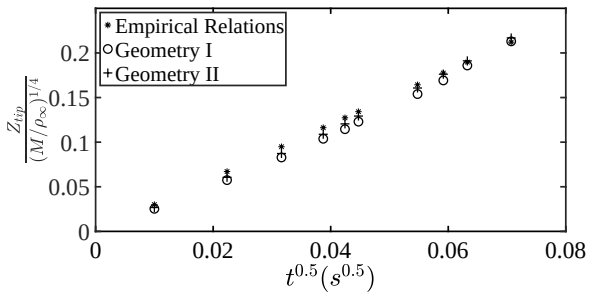

Figure 2: Self similarity of jet penetration length NPR=8.5

We now analyse the transient flow structures in the simulated cases. Figure 3 shows the Mach number field for both geometries when $NPR = 8.5$. The flow is choked at the nozzle exit ($Ma \approx 1$) and the so-called Prandtl-Meyer expansion fans can be observed just downstream of the nozzle exit, which lead the flow to become hypersonic. They extend to the jet boundary and are then reflected as intercepting oblique shock waves. 10μs ASOI, acceleration of the flow due to the produced sound waves

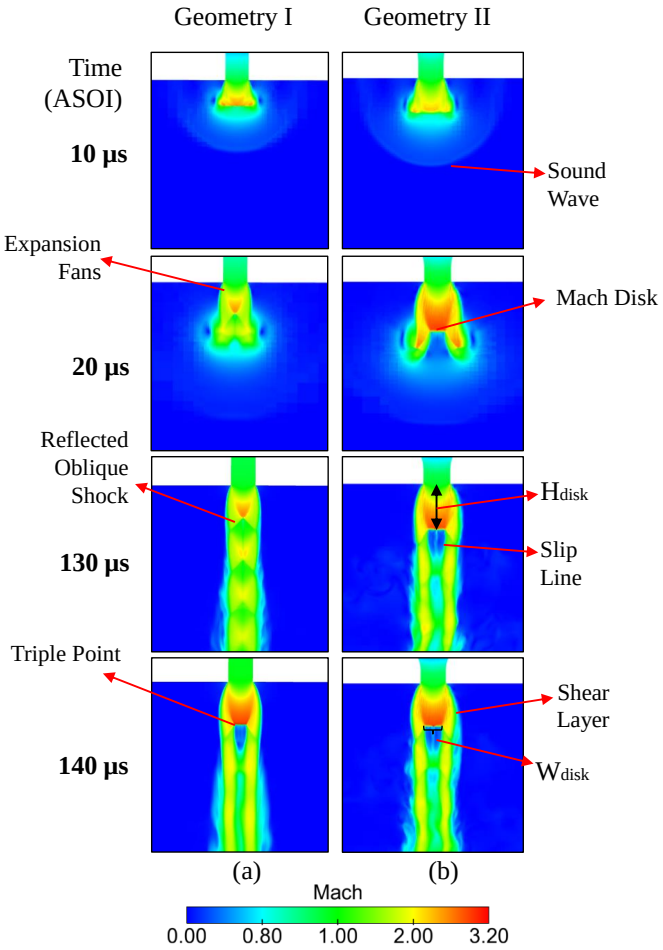

Figure 3: Triple point formation for $P_0 = 8.5$ bar with $P\infty = 1$ bar

is evident. Furthermore, 20μs ASOI initial tip vortices are bent towards the outer region of the jet and help methane/nitrogen mixing. Accumulation of compression oblique shock-waves slightly bent in towards the strong normal shock wave, referred to as the Mach disk. The flow behind the Mach disk is hypersonic ($Ma >> 1$) and it becomes subsonic ($Ma < 1$) after the Mach disk. The intersection between the closest oblique shock wave to the nozzle, the reflected oblique shock wave and the Mach disk is called the triple point. After the triple point, the slip line is formed so that the flow between slip line and reflected shock is supersonic ($Ma >> 1$) due to the expansion fans. The flow between the jet boundary and expansion fans is called shear layer which is where nitrogen are mixed. The findings presented in Fig. 3 are consistent with those reported in Refs. [5, 6] and [14, 15].

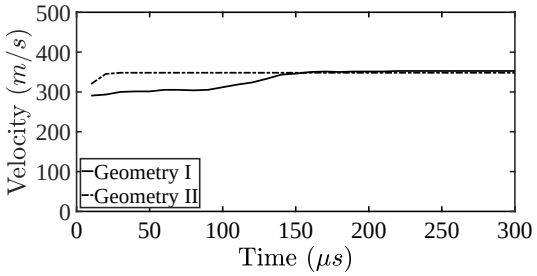

(a) Velocity

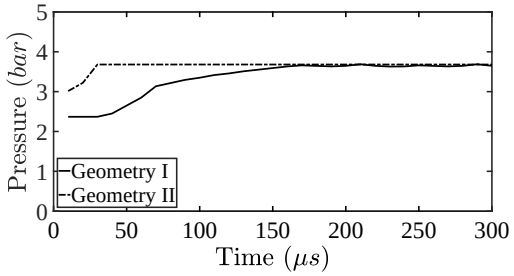

(b) Pressure

Figure 4: Development of Gaseous jet at Nozzle exit; $NPR = 6.5$

In Geometry I, the formation of the Mach disk and the triple pint took $120\mu s$ longer than that in Geometry II. In order to explore the reason behind this, the development of flow at the nozzle exit is investigated. The spatially averaged velocity and pressure at the nozzle exit is recorded as depicted in figure 4. As can be seen it takes $120\mu s$ to reach a constant pressure and velocity in Geometry II whereas it only takes $20\mu s$ to reach this condition for Geometry II. This is mainly due to having a longer tube connecting the high pressure tank to the main chamber in Geometry I which postponed the development of flow. It is therefore evident that the internal geometry can have an important influence on the transient process of jet development.

Conclusions

This study focused on developing a verification methodology to investigate the performance of LES in simulating highly underexpanded CNG jets using CONVERGE CFD.

The present work showed that the dominant flow features downstream of the gaseous jet such as Mach disk location, Mach disk width, triple point formation and penetration length, are consistent with those observed in previous studies. In addition, this work found that the internal geometry has a significant impact on the flow development at the nozzle exit and consequently, it affects the flow characteristics downstream of the gaseous jet. Our future work will focus on the effect of internal flow on the gas jet features using a more realistic injector geometry.

Acknowledgements

This research was supported by the Ford Motor Company and the Australian Research Council (ARC).

References

[1] Akira, Y. and Kiyosi, H., A Statistically-Derived Subgrid-Scale Kinetic Energy Model for the Large-Eddy Simulation of Turbulent Flows, *Journal of the Physical Society of Japan*, **54**, 1985, 2834–2839.

[2] Crist, S., Sherman, P. M. and Glass, D. R., Study of the highly underexpanded sonic jet., *AIAA Journal*, **4**, 1966, 68–71.

[3] Donaldson, C. D. and Snedeker, R. S., A study of free jet impingement. Part 1. Mean properties of free and impinging jets, *Journal of Fluid Mechanics*, **45**, 1971, 281–319.

[4] Dong, Q., Li, Y., Song, E., Yao, C., Fan, L. and Sun, J., The characteristic analysis of high-pressure gas jets for natural gas engine based on shock wave structure, *Energy Conversion and Management*, **149**, 2017, 26–38.

[5] Hamzehloo, A. and Aleiferis, P. G., Large eddy simulation of highly turbulent under-expanded hydrogen and methane jets for gaseous-fuelled internal combustion engines, *International Journal of Hydrogen Energy*, **39**, 2014, 21275–21296.

[6] Hamzehloo, A. and Aleiferis, P. G., Gas dynamics and flow characteristics of highly turbulent under-expanded hydrogen and methane jets under various nozzle pressure ratios and ambient pressures, *International Journal of Hydrogen Energy*, **41**, 2016, 6544–6566.

[7] Hill, P. G. and Ouellette, P., Transient turbulent gaseous fuel jets for diesel engines, *Journal of Fluids Engineering*, **121**, 1999, 93–101.

[8] Issa, R. I., Gosman, A. D. and Watkins, A. P., The computation of compressible and incompressible recirculating flows by a non-iterative implicit scheme, *Journal of Computational Physics*, **62**, 1986, 66–82.

[9] Khan, M. I., Yasmin, T. and Shakoor, A., Technical overview of compressed natural gas (CNG) as a transportation fuel, *Renewable and Sustainable Energy Reviews*, **51**, 2015, 785–797.

[10] Li, X., Christopher, D. M., Hecht, E. S. and Ekoto, I. W., Comparison of two-layer model for hydrogen and helium jets with notional nozzle model predictions and experimental data for pressures up to 35 MPa, *International Journal of Hydrogen Energy*, **42**, 2017, 7457–7466.

[11] Pomraning, E. and Rutland, C. J., Dynamic One-Equation Nonviscosity Large-Eddy Simulation Model, *AIAA Journal*, **40**, 2002, 689–701.

[12] Richardson, K. J., Senecal, P. and Pomraning, E., Converge 2.4.0 Theory Manual, Technical report, Madison, WI, 2017.

[13] Scarcelli, R., Wallner, T., Matthias, N., Salazar, V. and Kaiser, S., Mixture Formation in Direct Injection Hydrogen Engines: CFD and Optical Analysis of Single- and Multi-Hole Nozzles, *SAE Int. J. Engines*, **4**, 2011, 2361–2375.

[14] Vuorinen, V., Wehrfritz, A., Duwig, C. and Boersma, B. J., Large-eddy simulation on the effect of injection pressure and density on fuel jet mixing in gas engines, *Fuel*, **130**, 2014, 241–250.

[15] Vuorinen, V., Yu, J., Tirunagari, S., Kaario, O., Larmi, M., Duwig, C. and Boersma, B. J., Large-eddy simulation of highly underexpanded transient gas jets, *Physics of Fluids*, **25**, 2013, 1–22.